Proceedings of FEDSM2007:
5th Joint ASME /JSME Fluids Engineering Conference
July 30-August 2, 2007, San Diego, CA, USA

FEDSM2007-37435

Gas Bubble Formation in Stagnant and Flowing Mercury

Mark Wendel — *wendelmw@ornl.gov*
Ashraf Ibrahim — *ibrahimaa@ornl.gov*
David Felde — *feldedk@ornl.gov*
Bernard Riemer — *riemerbw@ornl.gov*

Oak Ridge National Laboratory[1], Oak Ridge TN, USA

ABSTRACT
The Oak Ridge National Laboratory's (ORNL) Spallation Neutron Source (SNS) facility uses a liquid mercury target that flows through a stainless steel containment vessel. As the SNS pulsed beam power level is increased, it is expected that the target vessel lifetime could become limited by cavitation damage erosion (CDE). Bubbles produced in mercury at an upwards-oriented vertical gas injector needle were observed with proton radiography (pRad) at the Los Alamos Neutron Science Center (LANSCE). The comparison of volume-of-fluid (VOF) simulation results to the radiographic images reveals some aspects of success and some deficiencies in predicting these high surface tension, highly buoyant, and non-wetting fluid behavior. Although several gas flows were measured with pRad, this paper focuses on the case with a low gas flow rate of 1.66 mg/min through the 0.2-mm-diameter injector needle. The acoustic waves emitted due to the detachment of the bubble and during subsequent bubble oscillations were also recorded with a microphone, providing a precise measurement of the bubble sizes. When the mercury is also motivated coaxially, the drag on the bubble forces earlier detachment leading to smaller bubble sizes.

1. INTRODUCTION
The Spallation Neutron Source (SNS) is an accelerator-based neutron source in Oak Ridge, Tennessee, USA. Within the year, this one-of-a-kind facility will provide the most intense pulsed neutron beams in the world for scientific research and industrial development [1]. Intense pulsed-proton-beam-induced heating of the SNS mercury target creates pressure waves that lead to the formation of cavitation bubbles in the mercury. Cavitation damage erosion (CDE) of the mercury container walls caused by violent collapse of these bubbles could potentially limit its power capacity and service lifetime [2]. Introducing a population of small gas bubbles into the mercury could lead to more effective damping of the beam-induced pressure waves. However, mercury, with its highly non-wetting characteristic on stainless steel and high surface tension is not well-suited to the formation and stabilization of small gas bubbles.

Kogawa et al. [3] experimented with X-rays to visualize gas bubble formation in stagnant mercury on a tiny needle with inner and outer diameters of 0.1 and 0.2 mm. They showed that the bubble formation in the low gas flow rate regime (where bubble size does not depend on flow rate) is a two-part process. In the first part, the bubble grows around the needle due to the non-wetting of the mercury on the needle material. In the second part, the buoyancy of the bubble overpowers the wall adhesion surface forces and the bubble rises and detaches. They were not equipped in their experiment to include the drag force on the forming bubble by flowing the mercury past the needle, but they speculated as to its effect on bubble size by calibrating a surface tension parameter from the stagnant tests, and assuming that it remains constant when the mercury is flowing.

By using the pRad facility[2] at LANSCE and the In-Beam Bubble Test Loop (IBBTL) developed at ORNL, this research on small mercury bubble formation could be advanced to include bubble formation in flowing mercury. A needle was mounted and tested in the IBBTL flow channel, and the formation and rise of the bubbles was visualized for various gas and mercury flow rates.

[1] Managed by UT-BATTELLE, LLC for the U.S. DEPARTMENT OF ENERGY under contract DE-AC05-00OR22725.
[2] This work has benefited from the use of the Los Alamos Neutron Science Center at the Los Alamos National Laboratory. This facility is funded by the US Department of Energy.

 Copyright © 2007 by ASME

More than 400 radiographs and several movies were taken during the pRad experiment including, many of which are relevant for the needle-bubbler investigation. Bubbles were observed for most test conditions. The smallest of these bubbles were between 200 and 300 micro-meters in diameter, while some of the larger bubbles were 3 or 4 mm. This paper is limited to discussion of one orientation (that where the needle is oriented upwards and the mercury flows upwards past the needle), and only for a low gas flow rate where the momentum of the incoming gas stream is not important to the developed bubble size.

Computational fluid dynamics was performed with CFX using the multiphase flow free-surface model for both axisymmetric and three-dimensional geometries. These efforts served to help assess the usefulness of the computational fluid dynamics (CFD) codes in designing gas/mercury systems.

NOMENCLATURE

D	=	Bubble diameter	mm
Q	=	Gas flow rate	ml/min
t_d	=	Bubble formation time	s
V_n	=	Velocity at needle tip	m/s

Greek symbols:

ρ_l	=	Mercury density	kg/m^3
μ	=	Dynamic viscosity	kg/(m–s)
σ	=	Surface tension	N/m

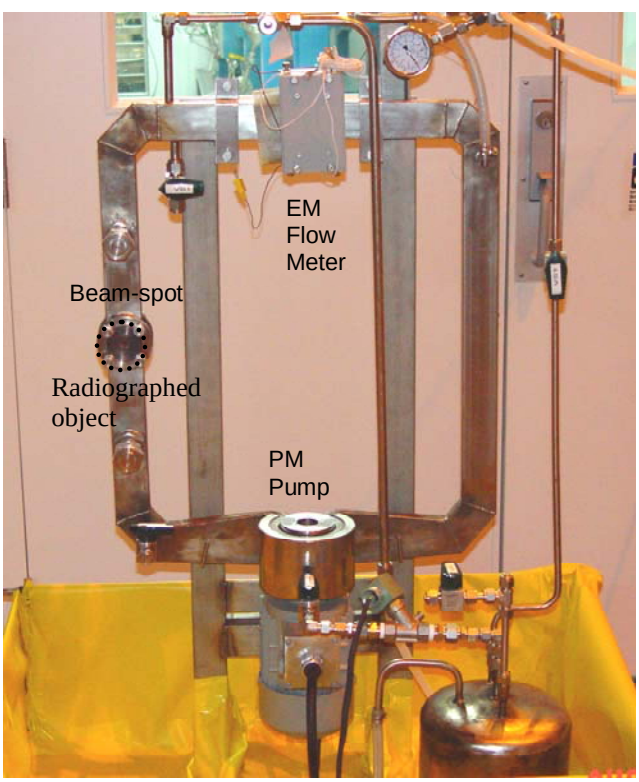

Figure 1. IBBTL loop used for pRad experiments.

2. EXPERIMENTAL APPARATUS

The IBBTL (Fig. 1) is oriented vertically and consists of a stainless steel channel with internal dimensions (22 mm × 48 mm) and a 1.5-mm wall thickness (Fig. 2). Mercury flow in the loop is motivated by a permanent magnet pump that is capable of reaching 1 m/s at the test section where the mercury is imaged. The flow rate is measured by an electromagnetic flow meter that requires the two electrodes to be in contact with the mercury.

The test flange (Fig. 3) holding the needle is inserted into a flange weldment located half-way up one side of the mercury loop (dashed circle in Fig. 1) , leaving a 6-mm mercury gap within which the needle is centered and directed upward. The center of the flange is 33 cm below the free surface at the top of the loop and the atmospheric pressure was 81 kPa during testing. The 25-mm-diam cylindrical base is inserted into the flow channel so that it represents an obstruction to the channel as shown in Fig. 2. The single-phase incompressible velocity distribution was computed with ANSYS-CFX [2] for this three-dimensional geometry and is shown in Figs. 4 and 5. The predicted mercury velocity at the tip of the needle, V_n, is 50% greater than the average channel velocity away from the test flange, which is measured by the flow meter. This ratio does not change appreciably for the two cases of V_n = 1.0 m/s and V_n = 0.65 m/s that were tested. As shown in Fig. 5, by the time a gas bubble travels 12.5 mm from the needle tip to the edge of the base circle, the mercury velocity will fall by only 8%.

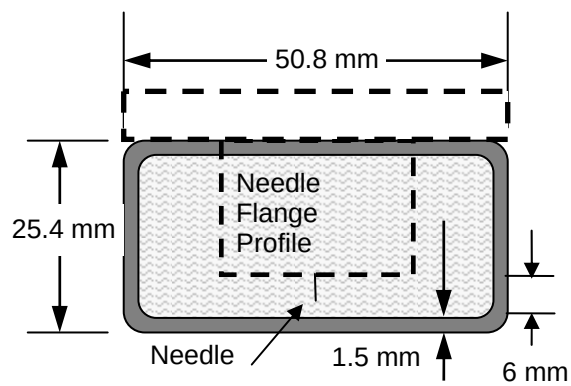

Figure 2. IBBTL channel cross-section.

The radiographic images were collected by a bank of cameras that were subdivided into three groups used to record images with time intervals between the groups of 360 μs and 340 μs, so there was a 700 μs spacing between the first and last image associated with each proton beam shot.

Before the radiographic tests were performed, the bubble size for each gas/mercury flow rate condition was measured with a microphone, which was attached to the outside wall of the

[2]ANSYS-CFX is a commercially available computational fluid dynamics solver developed by ANSYS, Inc., Southpointe, 275 Technology Drive, Canonsburg, PA 15317.

Copyright © 2007 by ASME

mercury channel. The sharp signals associated with bubble detachment frequency were clearly discernable.

3. EXPERIMENTAL DATA

The acoustic data are shown for the 1.66 mg/min cases in Table 1. For constant gas flow rate, the bubble diameter is calculated by

$$D = \left(\frac{6Qt_d}{\pi}\right)^{\frac{1}{3}} \qquad (1)$$

Where t_d is the bubble generation time, i.e. the period measured between successive detachments. A sample trace from the microphone signal is shown in Fig. 3.

As expected, the bubble size is less as the mercury velocity in the channel is increased. Typical radiographs for the four mercury flow rates are shown in Figs. 6–9. Here the bubble sizes can be confirmed, and for the larger bubbles which are created in the stagnant mercury (Fig. 6), the needle tip can be located within the bubble. The needle image is subtracted out from the image during image processing but the location of the tip can be located with figures like Fig. 9, where the bubble size is small.

Knowing the bubble period, the bubble velocity is calculated for each radiograph by measuring the average distance between the centroids of successive bubbles. Table 2 shows these results. The velocities for the cases with flowing mercury are dominated by the advection of the bubble and confirm the CFD, but for the stagnant mercury case, this velocity represents the rise velocity due to buoyancy.

Using the composite camera sub-group images it is possible to measure the bubble displacement during the 700 μs that elapse between the first and last images for each beam-shot. Fig. 10 shows the results of this method as applied for the 1 m/s case. Here the velocities of different features in the radiograph are indicated. The large bubble in Fig. 10 and bubbles on the side of the viewing area are entrained gas bubbles that are being circulated around the flow loop.

Figure 11 shows the formation and rise of a bubble under stagnant mercury conditions. Here the two-stage formation process is evident. The bubble grows downward away from the tip of the needle until it becomes buoyant enough to rise and detach from the needle.

2. SIMULATIONS

The numerical simulations were carried out using ANSYS-CFX version 11 with the homogeneous free surface model. The Volume of Fluid model (VOF) is specifically designed to track the position of a free surface between two immiscible phases and solves an additional advection equation for the additional phase. In the VOF model, a single set of equations is shared by the fluids, and the volume fraction of each of the fluids in each computational cell is tracked throughout the domain. The continuum surface force (CSF) proposed by Brackbill et al. [4] is used for the surface tension model. The additional surface tension model for the VOF calculation results in a source term in momentum equations

Table 1. Measured bubble size based on acoustic emissions from bubble detachment for helium flow of 1.66 mg/min.

Mercury Flow Velocity, V_n (m/s)	t_d (ms)	Equivalent Bubble Diameter (mm)
Stagnant	44	2.2
0.38	4.6	1.06
0.65	2.1	0.82
1.0	1.5	0.72

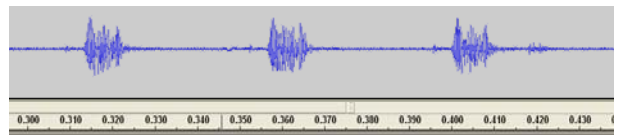

Figure 3. Oscilloscope trace for bubble generation in stagnant mercury.

Table 2. Rate of movement of helium bubbles based on the spacing between successive bubbles.

Mercury Flow Velocity, V_n (m/s)	t_d (ms)	Bubble Velocity (m/s)
Stagnant	44	0.22
0.38	4.6	0.37
0.65	2.1	0.65
1.0	1.5	1.00

and is expressed as volume force. The numerical scheme for the inclusion of this surface tension force has changed between ANSYS-CFX versions 10 and 11, and it was found that the scheme for version 10, although much slower, was more accurate. The problem with the version 11 scheme is not known, but it is manifested by nonphysical surface tension forces that appear on partition boundaries (for parallel processing runs). The wall adhesion model was invoked with a specified contact angle for the mercury of 133º.

Transient, turbulent, two-dimensional axisymmetric simulations have been completed for the flowing mercury cases. The SST turbulence model was invoked since the Reynolds number (3.8×10^4 to 1.0×10^5) indicates a fully turbulent regime. The axisymmetric case for stagnant mercury could not be completed due to nonphysical behavior at the centerline. The results for velocities of 0.38 and 1.0 m/s are shown in Fig. 12. The bubble sizes for the 0.38 m/s case were 1.2, 1.2, and 1.1 mm (only three bubbles simulated). For the 1.0 /s case, the average bubble size calculated was 0.70 mm.

Copyright © 2007 by ASME

These sizes are very close to the measured sizes, but the coalescence that occurred at the needle tip is not seen in the experiment, and the bubbles are much more elliptical in the radiographs.

For these 2D axisymmetric cases, both front and rear boundary surfaces of the wedge have been declared as symmetry. The outer wall of the cylinder and the bottom wall have been defined as walls with no slip condition. Buoyancy was included in the simulations with a reference density equal to that of the mercury. The time step used in this study was adapted to satisfy convergence criteria of 2×10^{-5}.

A three-dimensional simulation of the bubble formation during stagnant mercury conditions was performed (Fig. 13). The computational effort was exorbitant (80 hours of wall-clock time for 1 ms simulated using 8 state-of-the-art AMD64 processors), so results are presented here only for simulation times of 1, 2, 5, and 11 ms. In this time, the first stage of the bubble formation is seen consistent with the data and the bubble has just begun to move upward. These simulations used the an input switch to revert to CFX version 10 surface tension numerics, since the version 11 default surface tension numerics, although much faster, led to unphysical results particularly on the partition boundaries in parallel runs.

4. RESULTS AND DISCUSSIONS

The experimental (and computational) results agree with the Xray images presented by Kogawa et al. in that there is a two-stage bubble formation. The first stage involves growing bubble around the needle, and the second follows as the buoyancy overcomes wall adhesion. The measured bubble size here is 2.2 mm for stagnant mercury, whereas Kogawa et al. measured 2.7 mm. This difference may be due to a different degree of surface wetting by the mercury on the stainless steel.

The Morton number (M) is 3.7×10^{-14} for mercury. The Weber number (We) and Bond number (B) for the stagnant mercury case are 0.75 and 0.084. The bubble radius is used as the length scale in these parameters, the surface tension, σ, is 0.482 N/m. For the cases where the mercury is flowing at 1 m/s, the channel Reynolds number is 10^5, so all of the flowing mercury cases are fully turbulent.

A correlation for terminal velocity of a bubble in mercury is reported by Mori [5]:

$$u_T = \sqrt{\frac{2\sigma}{\rho_l D} + \frac{gD}{2}} = 0.21 \text{ m/s}$$

The terminal velocity in stagnant mercury (Table 2) agrees with Mori's findings.

The single phase predictions by ANSYS-CFX are found to be very accurate. However, multi-phase calculations have problems with stability and non-physical results probably exacerbated by mercury's high surface tension.

5. ACKNOWLEDGMENTS

The support from several LANSCE groups was greatly appreciated by the experimenters, including LANSCE-NS, pRad, IH, HP and Waste Services.

REFERENCES

1. www.sns.gov
2. Haines, J.R., Riemer, B.W., Felde, D.K., Hunn, J.D., Pawel, S.J. and Tsai, C.C., "Summary of Cavitation Erosion Investigations for the SNS Mercury Target", Journal of Nuclear Materials, vol. 343, pp. 58–69, 2005.
3. Kogawa, H., Shobu, T., Futakawa, M., Bucheeri, A., Haga, K., and Noaoe, T., "Effect of Wettability on Bubble Formation at Gas Nozzle Under Stagnant Condition," Proc. IWSMT-8, International Workshop on Spallation Materials Technology, Oct. 16-20, 2006, Taos, New Mexico.
4. Brackbill J.U., Kothe D.B., and Zemach, C., "A Continuum Method for Modeling Surface Tension", J Comp Phys, vol. 100, pp. 335–354, 1992.
5. Mori, Y., Hijikata, K., Kuriyama, K., 1977, "Experimental Study of Bubble Motion in Mercury with and without a Magnetic Field," J. Heat Transfer (Trans. ASME) 99, 404-410.

Copyright © 2007 by ASME

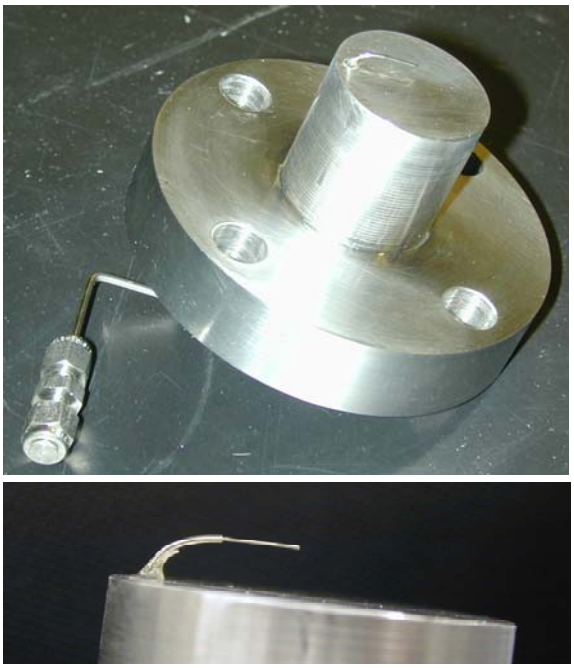

Figure 3. Close-up of needle-bubbler flange (top) and needle (bottom).

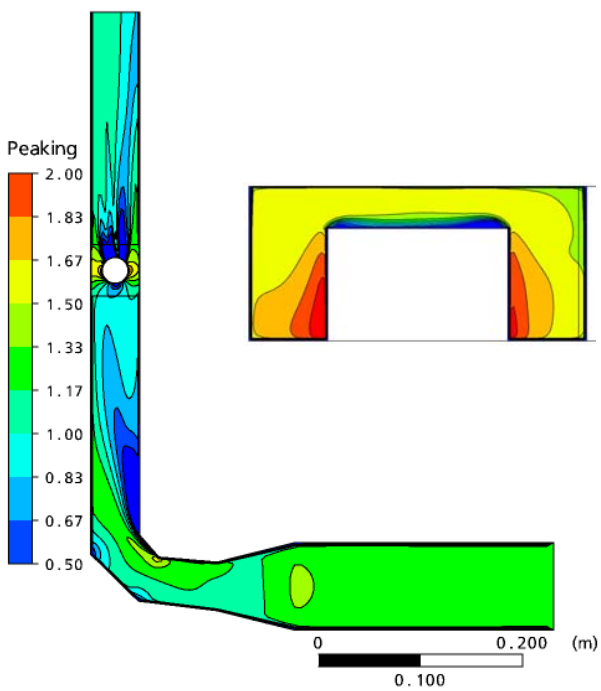

Figure 4. Predicted velocity profile in the IBBTL with the re-entrant needle flange inserted.

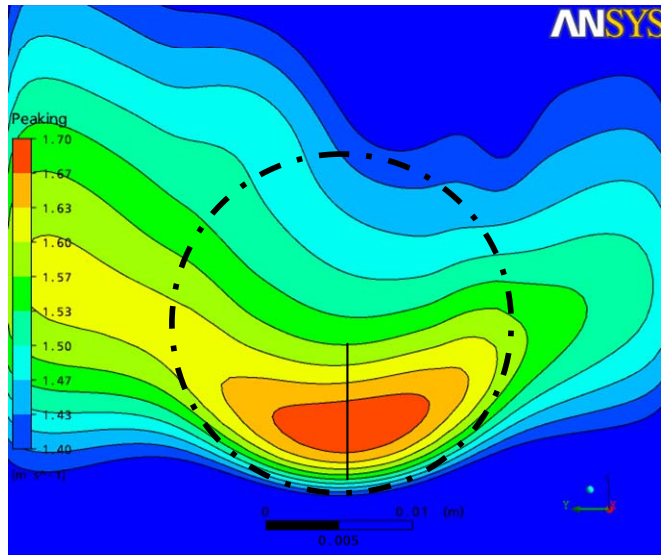

Figure 5. Predicted velocity profile in the vertical plane containing the needle.

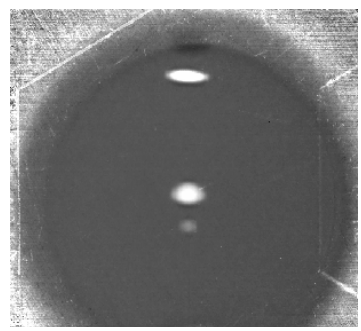

Figure 6. Stagnant mercury with 1.66 mg/min helium flow.

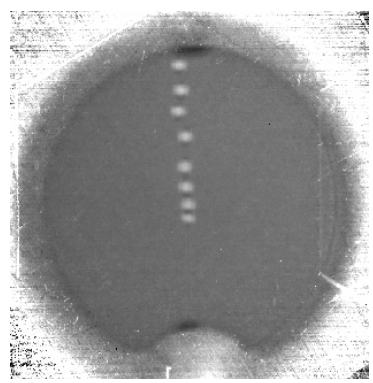

Figure 7. Mercury velocity is 0.38 m/s with 1.66 mg/min helium flow.

Copyright © 2007 by ASME

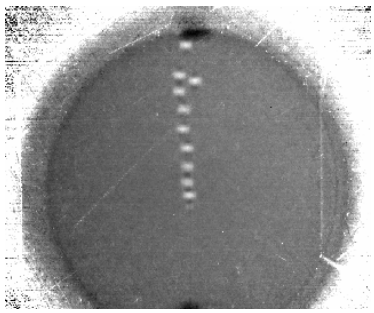

Figure 8. Mercury velocity is 0.65 m/s with 1.66 mg/min helium flow.

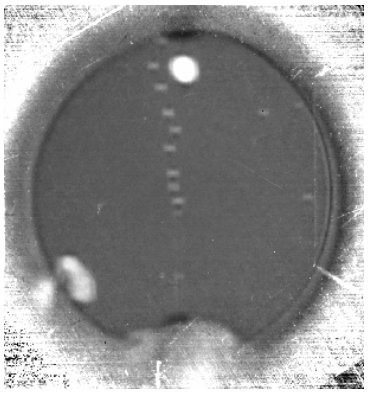

Figure 9. Mercury velocity is 1.0 m/s with 1.66 mg/min helium flow.

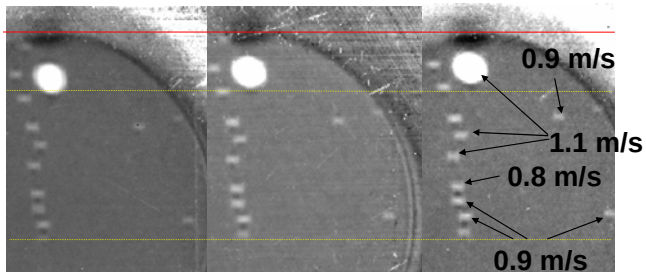

Figure 10. Velocity measurements of moving bubbles with the 1 m/s mercury condition.

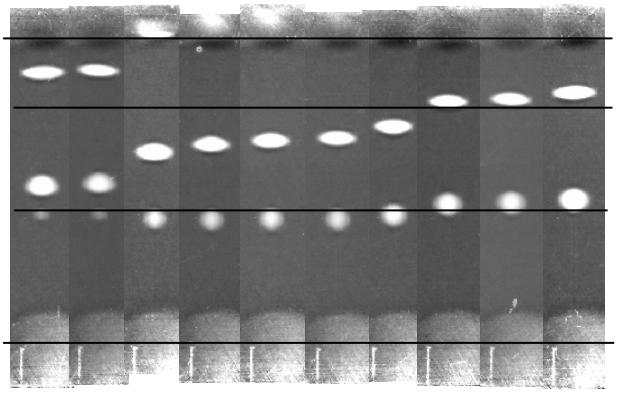

Figure 11. Formation and rise of helium bubble for stagnant mercury.

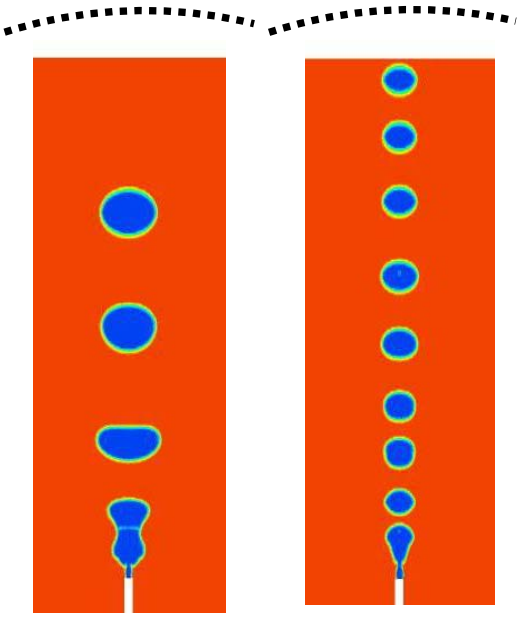

Figure 12. Axisymmetric CFX result for a mercury flow velocity of 0.38 m/s (left) and 1.0 m/s (right). Dashed line indicates the relative location of the base circle.

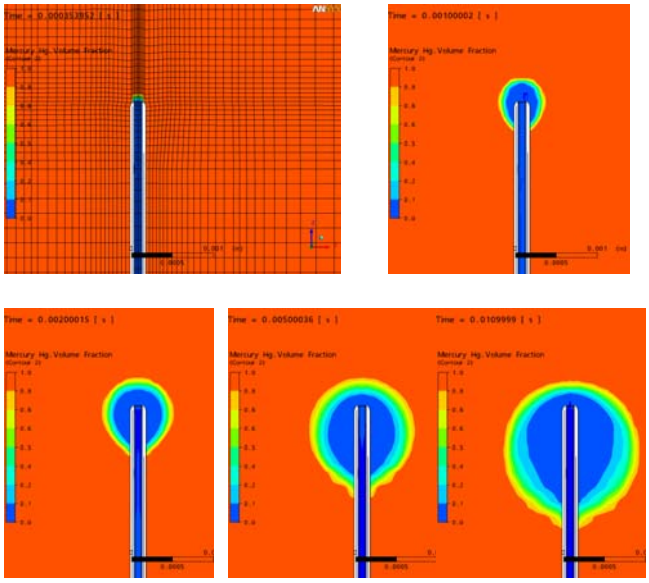

Figure 13. Three-dimensional CFX result for bubble formation in stagnant mercury.

Copyright © 2007 by ASME